Aerosol dynamics and gas-particle conversion in dry deposition of inorganic reactive nitrogen in a temperate forest

Genki Katata[1], Kazuhide Matsuda[2], Atsuyuki Sorimachi[3], Mizuo Kajino[4], and Kentaro Takagi[5]

[1]Institute for Global Change Adaptation Science (ICAS), Ibaraki University, Ibaraki, 310-8512, Japan
[2]Tokyo University of Agriculture and Technology, 3-5-8 Saiwai-cho, Fuchu, Tokyo 183-8509, Japan
[3]Department of Radiation Physics and Chemistry, Fukushima Medical University, 1 Hikarigaoka, Fukushima, Fukushima 960-1295, Japan
[4]Meteorological Research Institute, Japan Meteorological Agency, Tsukuba, Ibaraki 305-0052, Japan
[5]Teshio experimental forest, Field Science Center for Northern Biosphere. Hokkaido University, Toikanbetsu, Horonobe, Hokkaido 098-2943, Japan

Correspondence: Genki Katata (genki.katata.mirai@vc.ibaraki.ac.jp)

Abstract. Although dry deposition has an impact on nitrogen status in the forest environments, the mechanism for high dry deposition rates of fine nitrate aerosols (NO_3^-) observed in forests remains unknown and is a potential source of error in chemical transport models. Here we developed a new multi-layer land surface model coupled with dry deposition and aerosol dynamics processes for a temperate mixed forest in Japan. The processes of thermodynamics, kinetics, and dry deposition for mixed inorganic aerosols are modeled by a triple-moment modal method. The new model overall reproduces observed turbulent fluxes above the canopy and vertical micrometeorological profiles, as well as inorganic mass and size-resolved total number concentrations within the canopy. Sensitivity tests revealed that the within-canopy evaporation of ammonium nitrate (NH_4NO_3) under dry conditions significantly enhances deposition flux for fine NO_3^- and NH_4^+ aerosols, while reducing deposition flux for nitric acid gas (HNO_3). A dry deposition scheme coupled with aerosol dynamics may be required to improve the predictive accuracy of chemical transport models for the surface concentration of inorganic reactive nitrogen.

1 Introduction

Dry deposition of inorganic reactive nitrogen gas (e.g., HNO_3 and NH_3) and aerosols (e.g., NO_3^- and NH_4^+) is one of the important pathways of nitrogen into forest ecosystems. Recent studies at forests in East Asia, where air pollutant emissions continue to increase (EANET, 2016), revealed that observed dry deposition flux of inorganic reactive nitrogen of fine NO_3^- was markedly higher than that expected from theory (Takahashi and Wakamatsu, 2004; Yamazaki et al., 2015; Honjo et al., 2016; Sakamoto et al., 2018; Nakahara et al., 2019). As long as physical deposition processes are dominant, the deposition velocities of SO_4^{2-} and NO_3^- aerosols are expected to be similar because both species exist in the same sub-micron size range (e.g., Wolff et al., 2011). However, Sakamoto et al. (2018) showed observed deposition velocity of NO_3^- as high as those of HNO_3 at a temperate mixed forest, using the relaxed eddy accumulation method (Matsuda et al., 2015). Nakahara et al. (2019) also observed a higher concentration gradient of fine NO_3^- than of fine SO_4^{2-} at a cool-temperate forest, using a thermodynamic equilibrium model to explain this difference by evaporation of NH_4NO_3 aerosols in the NH_4NO_3-NH_3-HNO_3 triad within

the canopy. Numerical studies of chemical transport models for the East Asian region have demonstrated that the models have overestimated total (gas + aerosol) nitrate concentration at many locations (Kajino et al., 2013; Shimadera et al., 2018; Morino et al., 2015; Sakurai et al., 2015). Despite the many uncertain factors (e.g., the emission inventory; grid resolution;

25   chemistry, physics, dynamics, and deposition modules), Shimadera et al. (2014) demonstrated that the surface concentration of total nitrate could be reproduced by increasing dry deposition velocity of HNO_3 by a factor of twenty, in reference to past numerical studies. Hence, the deposition velocity of NO_3^- of fine aerosols and/or HNO_3 is among the major uncertainties in the chemical transport modeling.

Modeling studies for dry deposition have demonstrated the importance of NH_4NO_3 volatilization during dry deposition of

30   gaseous and particulate nitrates (Brost et al., 1988; van Oss et al., 1998; Kramm and Dlugi, 1994). All these studies used the "big-leaf" concept for the canopy representation under steady-state and thermodynamic equilibrium assumptions, with chemical reaction rates provided by observational data. Nemitz and Sutton (2004) developed a more sophisticated model by introducing chemical timescales for a size-resolved aerosol, and showed that the gas-particle conversion of NH_4NO_3 may explain the bi-directional fluxes observed above a Dutch heathland. However, several uncertainties remained in their model

35   results due to uncertainties in empirical treatments of aerosol deposition and thermodynamic processes, and gas concentration assumed in equilibrium with the aerosol phase of pure NH_4NO_3 (Nemitz and Sutton, 2004). Meanwhile, the equilibration of aerosols with surrounding liquid water is also important in determining the thermodynamic equilibrium of aerosols (e.g., Fountoukis and Nenes, 2007). An accurate evaluation of the impact of the NH_4NO_3-NH_3-HNO_3 conversion within the canopy requires a process-based model that includes the thermodynamics of mixed inorganic aerosols, linking to gas-phase chemistry,

40   while making no equilibrium assumption is required (Nemitz, 2015).

We here propose a new multi-layer land surface model coupled with dry deposition and aerosol dynamics (thermodynamics and kinetics of mixed inorganic aerosols) for forest environments. In aerosol dynamics modeling, the moment method is used to reduce computational cost and include general processes such as condensation, coagulation, below-cloud scavenging processes (e.g., Binkowski and Shankar, 1995), and dry deposition (Bae et al., 2009). These processes are implemented into a multi-layer

45   atmosphere-SOiL-VEGetation model (SOLVEG) that includes particle (aerosol and fog droplet) deposition and hygroscopic aerosol growth processes (Katata et al., 2014). We apply the model to a Japanese mixed forest for calibration and validation. Finally, we use numerical experiments to examine the impacts of two key processes on dry deposition flux over the canopy; gas-particle conversion of inorganic nitrogen compounds and hygroscopic growth.

2   Model description

50   ### 2.1   Model overview

A one-dimensional multi-layer model SOLVEG model consists of four sub-models: atmosphere, soil, vegetation, and radiation within the vegetation canopy. The general description for gas and particle transport and dry deposition is available in Katata and Ota (2017). In the atmosphere sub-model, one-dimensional diffusion equations are solved between atmospheric layers for horizontal wind speeds, potential temperature, specific humidity, liquid water content of the fog, turbulent kinetic energy

55 and length scale (Katata, 2009), and gas and aerosol concentrations (Katata and Ota, 2017). Observational data are used for
the upper boundary conditions. Bulk transfer equations are applied at the lowest layer using the soil surface temperature and
specific humidity calculated in the soil sub-model.

In the soil sub-model, the soil temperature, volumetric soil water content, and soil pore specific humidity are respectively
predicted from heat conduction, mass balance in liquid water, and water vapor diffusion equations, respectively (Katata, 2009).
60 Root water uptake is calculated from the transpiration rate in the vegetation sub-model. For soil CO_2, mass conservation
equations for liquid and gas phases are solved (Nagai, 2004). Organic matter dynamics are also considered (Ota et al., 2013);
microbial decomposition and dissolved organic carbon (DOC) leaching in the above-ground litter layer, below-ground input
of carbon from roots (root litter), and soil organic carbon (SOC) turnover and DOC transport along water flows throughout the
soil profile for three SOC pools (active, slow, and passive) with different turnover times.

65 In the vegetation sub-model, profiles are predicted for leaf temperature, leaf surface water, and vertical liquid water flux
(Nagai, 2004). The heat budget equation at the leaf surface is solved to predict leaf temperature using key variables from the
atmosphere sub-model combined with the radiation scheme. At the upper boundary of the sub-model, a given precipitation
intensity is used for calculating vertical liquid water flux within the canopy based on the surface water budget equation. The
CO_2 assimilation rate due to photosynthesis is predicted using Farquhar's formulations (Farquhar et al., 1980) and stomatal
70 resistance. In the radiation sub-model, direct and diffuse downward and upward fluxes of solar and long-wave radiation are
calculated to obtain the radiation energy input at the canopy layers. Fractions of sunlit and shaded leaves at each canopy layer
are adopted for the stomatal resistance and energy budget calculations.

A multi-layer snow module is unique in including the gravitational and capillary liquid water flows in the unsaturated snow
layer based on van Genuchten's concept of water flow in the unsaturated zone (Katata et al., submitted). In the soil module, soil
75 freeze-thaw processes based on the freezing-point depression equation are considered in heat conduction and liquid water flow
equations. Winter-related processes for grassland phenology, such as leaf development and senescence due to cold stresses,
are also implemented in the vegetation sub-model. Carbon gain from photosynthesis and remobilized reserves are allocated
among sinks based on changing sink priorities and strengths. Sink strengths are calculated based on the dynamics of leaves and
stems and the acclimation to low temperature. The removal of tillers and leaves by cutting can be simulated during the growing
80 season, with subsequent regrowth of the sward. The regrowth rate after cutting is calculated at each phenological stage. Natural
turnover of leaves and roots is modeled using typical life spans in years. Rooting depth and the fraction of roots in soil layers
are modeled as functions of root biomass. Daily amounts of the dead root biomass (root litter) are used as inputs to SOC in the
soil sub-model of SOLVEG.

2.2 Dry deposition

85 Since full descriptions for the dry deposition process of gases and particles are available in Katata et al. (2013; 2014) and
Katata and Ota (2017), only the key equations are presented in the present subsection.

Using the compensation points for trace gases in the sub-stomatal cavity, χs (nmol m^{-3}), and above the leaf water surface, χ_d (nmol m^{-3}), we model bi-directional gas exchange fluxes over stomata, F_{gs} (nmol m^{-2} s^{-1}), and over leaf water surfaces, F_{gd} (nmol m^{-2} s^{-1}), for each canopy layer (Katata et al., 2013) as follows:

90
$$F_{gs} = a(D_{gas}/D_w)R^{^{\backprime}-1}[(r_b + r_d)\chi_s - r_b\chi_d - r_d\chi_a], \tag{1}$$
$$F_{gd} = a(D_{gas}/D_w)R^{^{\backprime}-1}[(r_b + r_s)\chi_d - r_b\chi_s - r_s\chi_a], \tag{2}$$

where D_{gas} and D_w are the diffusivities (m^2 s^{-1}) of trace gas and water vapor, r_a and r_s are the resistances (m s^{-1}) of leaf boundary layer and stomata, and χ_a is the ambient gas concentration (nmol m^{-3}) in the canopy layer. The total gas exchange flux over the leaves can be calculated as the sum of F_{gs} and F_{gd} for all canopy layers. In accordance with a number
95 of observations (e.g., Huebert and Robert, 1985), all χ_s, r_d, and r_s are set to be zero for highly reactive and water-soluble gas species of HNO$_3$ and HCl, i.e., perfectly absorption by plant canopies. For both species, the parameterization for a deciduous forest by Meyers et al. (1989) is used to calculate r_b. For NH$_3$, χ_s is calculated based on the thermodynamic equilibrium between NH$_3$ in the liquid and gas phases:

$$\chi_s = \frac{161500}{T_c}\exp\left(\frac{10378}{T_c}\right)\Gamma_s, \tag{3}$$

100 where χ_s is the stomatal emission potential (also known as the apoplastic ratio) at 1013 hPa. The NH$_3$ concentration at the leaf surface water (χ_d) is calculated by assuming Henry's Law and dissociation equilibrium with the atmospheric concentration of NH$_3$ at each canopy layer. To calculate the exchange flux of SO$_2$ and NH$_3$ over the wet canopy, the following formula for the evaporation (cuticular) resistance (r_d) is applied:

$$r_d = 31.5AR^{-1}\exp[a(100 - RH)], \tag{4}$$

105 where RH is the relative humidity (%) and AR is the ratio of total acid/NH$_3$, represented as $(2[SO_2] + [HNO_3] + [HCl])/[NH_3]$ at each atmospheric layer. The value of AR is determined from calculations of gaseous inorganic concentration at each atmospheric layer. Since the affinity of SO$_2$ for the leaf surface is approximately twice that of NH$_3$ (van Hove et al., 1989), a half value of r_d calculated by Eq. (4) is applied to SO$_2$ deposition.

As explained in Katata et al. (2014), the aerosol deposition rate F_p (μg m^{-2} s^{-1} or # m^{-2} s^{-1}) of each inorganic species in
110 each canopy layer is represented as

$$F_p = aE_p, \tag{5}$$
$$E_p = \varepsilon F_f|\mathbf{u}|c_p, \tag{6}$$

where E_p is the capture of aerosols by leaves (μg m^{-3} s^{-1} or # m^{-3} s^{-1}); ε the total aerosol capture efficiency of plant leaves for aerosols by inertial impaction, gravitational settling, Brownian diffusion, and interception; F_f is the shielding coefficient

115 for aerosols in the horizontal direction; $|\mathbf{u}|$ the horizontal wind speed (m s^{-1}) at each canopy layer; and c_p is the mass or number concentration of aerosols (μg m^{-3} or # m^{-3}).

2.3 Aerosol dynamics

In order to simulate changes in aerosol particle sizes due to condensation, evaporation, and water uptake, a triple-moment modal method (Kajino et al., 2012) is employed at each atmospheric layer in SOLVEG. Aerosols are grouped into fine (accumulation)

120 and Aitken mode with the size distribution prescribed by a lognormal function; while the coarse mode is not considered in the simulation. The lognormal function is identified by three parameters: number concentration (N [# m^{-3}]), geometric mean diameter (D_g [μm]), and geometric standard deviation (σ_g). The triple-moment method predicts spatiotemporal changes in three moments to identify the changes in the shape of each mode's lognormal size distribution. The selected three moments are 0th, 2nd, and 3rd moments (M_0, M_2, and M_3), which are respectively number (N), surface area (m^2 m^{-3}), and volume

125 concentrations (m^3 m^{-3}). D_g values for each moment are named D_{g0}, D_{g2}, and D_{g3}. The relationship of the above lognormal parameters and the three moments for each atmospheric layer are as follows:

$$M_k = N D_{g0}^k \exp\left[\frac{k^2}{2}\ln^2\sigma_g\right], \tag{7}$$

$$D_{g0} = \left[\frac{M_2}{M_0}\right]^{\frac{3}{2}}\left[\frac{M_3}{M_0}\right]^{-\frac{3}{2}}, \ln^2\sigma_g = -\ln\left[\frac{M_2}{M_0}\left(\frac{M_3}{M_0}\right)^{-\frac{2}{3}}\right]. \tag{8}$$

Aerosol growth is dynamically solved in the same manner of Kajino et al. (2012). The gas to aerosol mass transfer is

130 accelerated by the difference between the current state and the thermodynamic equilibrium state, as simulated by ISORROPIA2 model (Fountoukis and Nenes, 2007) for semi-volatile inorganic components such as NO$_3^-$, NH$_4^+$, Cl$^-$, and liquid water (H$_2$O). The gas-particle conversion of organics is not considered in the present study because the observational speciation data was not available. Thus, both organics and other components to total mass was assumed to be hydrophobic aerosols in the simulation. Since the current study focuses on change in mass gain/loss of accumulation mode aerosols, coagulation processes are not

135 included in the simulation. Brownian coagulation is critically important for the prediction of number concentration of Aitken mode aerosols, but not very important for the prediction of accumulation mode aerosol mass (e.g., Kajino et al., 2013).

3 Simulation setup

3.1 Study site and observational data

We used the measurements at an observation tower in a mixed forest namely the Field Museum Tamakyuryo (FM Tama) of

140 Tokyo University of Agriculture and Technology, located in a western suburb of Tokyo, Japan (35°38'N, 139°23'E). Deciduous tree species (*Quercus* spp.) are dominant around the meteorological tower along with some Japanese cedar (*Crytomeria*

japonica). The canopy height around the tower is approximately 20 m. The growth period of deciduous trees is typically from April to December. Site description details are provided by Matsuda et al. (2015) and Yamazaki et al. (2015).

Simulations were carried out in two experimental periods in the early autumn (26 September to 11 October 2016) and the
145   late autumn (7 November to 7 December 2016). In the early autumn period, daytime (8:00–17:00 in local time) and nighttime (17:00–8:00 in local time) mean concentrations were available at five heights (1, 8, 16, 23, and 30 m) for inorganic gases, with fine aerosol concentrations observed using a 4-stage filter-pack sampling system. System specifications were same as those of Nakahara et al. (2019) except for the aerosol filter material. This study used a grass fiber filter coated with Teflon for collecting fine and coarse aerosols. Sampling was continuously performed during the day and night except when it was raining.
150   We obtained 5 daytime reading data sets and 6 nighttime reading data sets. After the samples were collected, inorganic ions in each of the filters were extracted into deionized water by ultrasonic extraction, and then analyzed using ion chromatography (Dionex ICS-1100, Thermo Scientific).

In the early autumn period, measurements of particle number concentrations were taken during the daytime (10:00 - 16:00) for 7 days without rainfall. Airborne particle number concentrations were measured by an electrical low pressure impactor
155   (ELPI+, Dekati Ltd.). In the ELPI+, sampled particles are charged by corona discharge and later separated by size using the principle of inertial classification in a 13-stage cascade low-pressure (40 hPa) impactor combined with a back-up filter stage. During the collection process, the charged particles produce a current proportional to their respective number concentrations. The broad particle size distribution domain measured by the ELPI+ ranges from 6 nm to 10 μm. More details on the ELPI+ are described in Järvinen et al. (2014). The aerosol sample inlets for the ELPI+ were placed at heights of 30, 23, 17, 8, and 1 m
160   at the tower through TYGON intake tubing of 7.94 mm inner diameter and respective lengths of 6, 5, 10, 20, and 25 m . Each sampling line for the 5 measuring heights was manually switched every two minutes. The transit times for aerosol samples in the tubing at each height ranged between 2 and 12 s. Results of the first minute of concentration measurement were rejected in order to avoid the mixing of air samples derived from different heights. All data were stored in a personal computer at a sampling rate of 1 s^{-1}. The raw data were averaged over intervals of 60 s and were later used for calculating 600 s mean vertical
165   profiles. Particle penetration efficiencies of the sampling tubes were estimated using the indoor aerosols in the laboratory by changing the lengths of the sampling tubes (30, 20, 15, 10, and 5 m). Based on these results, the raw concentrations have been corrected prior to post-processing. Furthermore, the data were further screened out according to a few selection criteria to ensure their credibility with respect to three uncertainties in particular: uncertainty in number concentration measurements, signal to noise ratio (Deventer et al., 2015), and variation in background current (the signal obtained from particle-free air
170   through a HEPA-filter for each particle stage) before and after the measurements.

Half-hourly meteorological data for horizontal wind speed, and air temperature and humidity at heights of 30, 25, 20, 10, 6, and 1 m at the tower were used for model input and validation. Incoming short-wave and long-wave radiation values at 30 m were used for model input, while the latter was estimated by the parameterization of Duarte et al. (2006). Net radiation was measured using a net radiometer (Q7, REBS) and stored by a data-logger (CR10X, Campbell Scientific) as half-hourly means.
175   A sonic anemometer (81000, Young) was used to measure the 3D wind velocities and air temperature, and an enclosed infrared CO_2/H_2O gas analyzer (LI-7200, Li-Cor) was used to measure the molar fraction of CO_2 and H_2O. These data were sampled at

a frequency of 10 Hz with the interface unit (LI-7550, Li-Cor). Half-hourly CO_2, heat, and momentum fluxes were calculated using Eddy Pro software (ver. 4.2.0, Li-Cor), where double rotation (Kaimal and Finnigan, 1994) and block averaging were applied to the fluctuation data to calculate the covariances. We then corrected the effect of air density fluctuations on the flux
180   values (Burba et al., 2012). Low-frequency losses (Moncrieff et al., 2004) and high-frequency losses for the low-pass filtering (Ibrom et al., 2007) and for the sensor separation (Horst and Lenschow, 2009) were corrected. All raw flux data were checked following the quality-control program proposed by Vickers and Mahrt (1997). Then we applied the quality check system proposed by Mauder and Foken (2006), and excluded data of low quality (qc-flag of 2).

The total (one-sided) leaf area index (LAI) measured with a plant canopy analyzer (LAI-2200, Li-cor) were 4.3 and 3.6
185   m^2 m^{-2} for October and November 2016, respectively. Vertical profiles of leaf area density (LAD) were provided in order to obtain the above values of total LAI by interpolated by gamma function interpolation, with the maximum at a height of 15 m following the way of Katata et al. (2013). LAI of the understory vegetation of 0.5 m in height was given as a typical value of 2.0 m^2 m^{-2} due to lack of observational data.

3.2   Boundary and initial conditions

190   The boundaries of the vegetation layers were set at heights of 0.05, 0.1, 0.2, 0.3, and 0.5 m (understory vegetation), and from 1 to 20 m (forest canopy) with an increment of 1 m, while atmospheric layers were extended from the 20 m canopy to 30 m with an increment of 1 m. Half-hourly data for precipitation, atmospheric pressure, horizontal wind speed, air temperature and humidity, and incoming long- and short-wave radiation were applied to the top atmospheric layer. Inorganic mass concentrations of gases (SO_2, NH_3, HNO_3, and HCl) and PM2.5 aerosols (SO_4^{2-}, NO_3^-, NH_4^+, Na^+, Cl^-, Ca^{2+}, K^+, Mg^{2+}) measured
195   by filter-pack were linearly interpolated at half-hourly timescales. For Aitken mode, the inorganic mass concentration was assumed to be one-tenth of that of fine mode, based on size-resolved number concentrations from ELPI+ observations (not shown in figures). The boundaries of the soil layers were 0.02, 0.05, 0.1, 0.2, 0.5, 1.0, and 2.0 m in depth. Constant values for soil temperature (15 °C) and saturated volumetric water content for typical loam soil texture (0.43 m^3 m^{-3}) were taken from Katata and Ota (2017).

200   The lognormal parameter sets of (D_{g3}, σ_g) for fine and Aitken modes at the upper boundary condition were respectively set at (0.089 μm, 2.1) and (0.26 μm, 2.0), based on observational results in urban environments in autumn (Salma et al., 2011). This size distribution was similar to that observed at a 30 m height by ELPI+ systems (Fig. 1a). The volume fraction of inorganic compounds, f_{io}, lacks an observational data basis, and was set at 0.2 and 0.12, respectively, for fine and Aitken modes, in order to simulate the total number concentration observed by ELPI+ measurements at a height of 30 m in the late autumn
205   period. Since no ELPI+ data are available for the early autumn period, temporal changes in f_{io} (Fig. 1b) were set based on the filter-pack data at the study site and total PM2.5 mass concentrations observed at the nearest air quality monitoring station at Hachiouji (3 km west-north-west from the site). f_{io} for Aitken mode was assumed to be the same as that for fine mode, since again no observational data were available. As a result, the summed volume for both organics and other components varied from 40 and 80 % of the total volume. Since no data were available in the study site for emission potentials of NH_3 at the

210 ground surface (χ_g) and stomata (χ_s), we used typical values of χ_g = 300 ppb (Massad et al., 2010) and χ_s = 2000 ppb for forests (Neirynck and Ceulemans, 2008).

3.3 Simulation scenarios

To reveal the impacts of each process of NH_4NO_3 equilibrium and hygroscopic growth, the following four simulation scenarios were adopted: 1) NH_4NO_3 equilibrium and aerosol water uptake ("gpc" scenario), 2) aerosol water uptake but no NH_4NO_3

215 equilibrium ("no gpc" scenario), 3) NH_4NO_3 equilibrium but no aerosol water uptake ("gpc dry" scenario), and 4) no NH_4NO_3 equilibrium and no aerosol water uptake ("no gpc dry" scenario). Calculations in all scenarios were compared with observations of vertical profiles of total number and inorganic mass concentrations within the canopy.

4 Results

4.1 Micrometeorology during autumn 2016

220 Temporal changes in friction velocity, net radiation, sensible and latent heat, and CO_2 flux over the canopy for the early autumn and the late autumn periods are shown in Fig. 2. Overall, the modeled momentum and heat fluxes agreed with observed values, while observed high values of friction velocity in November and December 2016 were slightly underestimated (Fig. 2f). Water vapor and CO_2 exchange processes that determine the level of stomatal uptake of gases were also reproduced well by the model (Fig. 2c, e, h, and j).

225 Figure 3 illustrates time series for horizontal wind speed, air temperature, and relative humidity under the canopy. Wind speed was underestimated within the forest, as was friction velocity (Fig. 3a and d), probably due to horizontal advection over the hilly terrain (Matsuda et al., 2015). Nevertheless, air temperature and humidity, the primary determinants of ambient conditions of gas-particle conversion and aerosol hygroscopic growth, were reproduced by the model (Fig. 3b, c, e, and f).

4.2 Inorganic mass concentration and flux in early autumn in 2016

230 Figure 4a and b shows time series for observed and calculated major inorganic nitrogen compounds (HNO_3 and NH_3 gases and NO_3^-, and NH_4^+ fine aerosols) under the canopy in the early autumn period. The difference between "gpc" and "no gpc" scenarios was substantial for HNO_3 and fine NO_3^- concentrations during the daytime on 28 September. In the "gpc" scenario, HNO_3 concentration increased due to evaporation of NH_4NO_3 during the daytime, while NO_3^- concentration decreased. As a result, strong variations in NO_3^- mass concentration was reproduced in the "gpc" scenario. Less impact of evaporation of

235 NH_4NO_3 on both fine NH_3 and NH_4^+ concentrations was observed.

The calculated fine mode mass-based wet diameter (D_{g3}) and RH are shown in Fig. 4c. Hygroscopic growth has a large impact on aerosol size distributions in comparisons between "no gpc" and "no gpc dry" scenarios; e.g., D_{g3} values in the latter were higher as 1.4 μm than those in the former as 0.4 μm during the nighttime on 29 September 2016. Although this process also influenced the size distribution during the daytime, a competing shrinkage mechanisms, NH_4NO_3 evaporation, appeared

240 in the "gpc" scenario. As a result, the difference in daytime D_{g3} between "gpc" and "no gpc" scenarios was up to in 0.12 μm on 28 September.

Figure 5 depicts vertical profiles of normalized gaseous and particulate mass concentrations in the early autumn period. In the "no gpc" scenario (Fig. 5b), vertical gradients of fine aerosol compounds (SO_4^{2-}, NO_3^-, and NH_4^+) were similar, since the same equations for deposition velocity of Eqs. (5) and (6) were used for all inorganic aerosol compounds. In contrast, vertical

245 gradients of NO_3^- and NH_4^+ concentrations drastically increased due to NH_4NO_3 evaporation in the "gpc" scenario (Fig. 5c and f), producing gradients similar to observed gradients (Fig. 5a and d). The impact of NH_4NO_3 evaporation was smaller during the nighttime (Fig. 5c) than the daytime (Fig. 5f), which also aligns with observed diurnal patterns (Fig. 5a and d). High values of observed fine SO_4^{2-} concentration were reproduced in both scenarios (Fig. 5a–c).

Figure 6 shows time series for calculated mass flux of HNO_3, NH_3, and fine NO_3^- and NH_4^+ over the canopy for "gpc" and

250 "no gpc" scenarios. The impact of NH_4NO_3 evaporation on fluxes was the highest from 26 to 29 September. Calculated NO_3^- flux above the canopy was positive during the nighttime for several days (Fig. 5c) due to condensation of HNO_3 (Fig. 5a). As is the case for in-canopy NH_3 concentration (Figs. 4 and 5), NH_4NO_3 evaporation has a less impact on NH_3 flux than other species (Fig. 6b).

4.3 Aerosol size distribution in late autumn 2016

255 Figure 7 shows time series for number concentration within the canopy in the late autumn period, as well as parameters for a lognormal size distribution for fine mode. Initial number concentration values on 7 November (Fig. 7a) were tuned via adjustments of the ratio of inorganic compounds (f_{io}) for each mode. Below-canopy D_{g3} and σ_g were smaller in "gpc dry" than in "no gpc dry" due to NH_4NO_3 evaporation (Fig. 7b and d), while below-canopy D_{g0} was larger in "gpc dry" than in "no gpc dry" (Fig. 7c). In the "gpc" and "no gpc" scenarios in which aerosol water is considered, D_{g3} increased due to

260 hygroscopic growth, while the influence of NH_4NO_3 equilibrium on D_{g3} was still apparent (Fig. 7b). Some discrepancies between observations and calculations were found after 25 November 2016 in temporal changes in number concentration (Fig. 7a).

Figure 8 shows vertical profiles of parameters for a lognormal size distribution and normalized NO_3^- mass concentration in "no gpc" and "gpc" scenarios. For fine aerosols, values of D_{g3} and normalized NO_3^- concentration at 8 m were respectively

265 5.1 % and 8.9 % smaller in the "gpc" scenario than in the "no gpc" scenario due to evaporation of NH_4NO_3 (Fig. 8b and d), while calculated σ_g was also 1.2 % smaller (Fig. 8c). In contrast, calculated D_{g0} slightly increased 0.3 % at the same height (Fig. 8a). Almost no effect of NH_4NO_3 equilibrium was found in Aitken mode (Fig. 8e-h).

Figure 9 shows the differences in the total number concentration among above, within, and below the canopy during the daytime in the late autumn period, with particular reference to the differences amoung these concentrations. In the sub-micron

270 size range (0.1 - 0.4 μm), differences between height pairs were strong between 8 and 1 m (below), between 30 and 24 m (above), and between 24 and 8 m (within). In the "no gpc dry" scenario, the difference in number concentration between height pairs was minimal in the sub-micron size range as determined by modelled size-resolved dry deposition velocity (Fig. 9e). In the "gpc" scenario (Fig. 9a–d), aerosols in fine mode shrunk in this size range due to in-canopy NH_4NO_3 evaporation, resulting

in an apparent tendency to emit from the canopy to the air above (Fig. 9d). Meanwhile differences in number concentration be-
tween 24 and 8 m (within) for large aerosols (> 0.3 μm) were excessively high in the "gpc" scenario compared to observational
data. In the "no gpc" scenario, in which only aerosol water uptake was considered (Fig. 9c), fine aerosol size increased due
to hygroscopic growth (Fig. 6), and the concentration differences between height pairs always remained positive in this range.
Finally, if the "gpc" scenario, in which both processes of NH_4NO_3 evaporation and hygroscopic growth are considered (Fig.
9b), calculated negative gradients of number concentration appeared between 24 and 8 m (within) for the sub-micron range
0.1-0.4 μm, again similar to the observed patterns (Fig. 9a).

5 Discussion

5.1 Uncertainties in model results

SOLVEG reproduced the general features of gas concentration, fine aerosol mass, and fine aerosol number concentration
observed within the canopy. Several uncertainties (e.g., low time resolution of weekly filter-pack data in the late autumn period;
complex topography of the study site) may cause underestimations in calculated wind speed (Fig. 3a and d) and overestimations
in total number concentration within the canopy after 25 November 2016 (Fig. 6a). In the modeling aspect, aerosol growth due
to biogenic secondary organics was not considered and might increase uncertainty in model results. Although this effect might
not be important for dry deposition and evaporation of NH_4NO_3 that was the main focus of this study, this effect certainly
influences the aerosol mass flux itself in the forest. Nevertheless, the order of the magnitude of observed normalized inorganic
mass concentration within the canopy during the daytime, i.e., SO_4^{2-} > NH_3 > NH_4^+ > NO_3^- > HNO_3 (Fig. 5a) was well
reproduced by the model in the "gpc" scenario (Fig. 5c). In the late autumn period, while there is no direct measurement of
aerosol water content, the ambient RH profile that determines hygroscopic growth of aerosols was reproduced (Fig. 3c and f).
As a result, the observed in-canopy negative gradient in number concentration (i.e., apparent emission of aerosols) in 0.1 - 0.4
μm size range was simulated in the "gpc" scenario (Fig. 9a and b). These results indicate that the model results can likely be
used to effectively address the impact of aerosol dynamics on dry deposition processes.

5.2 Formation mechanisms of aerosol size distributions

The complex form of the aerosol size distribution can be mainly explained by the combination of (1) effects of in-canopy
NH_4NO_3 evaporation of small aerosols and (2) fine mode hygroscopic growth of large aerosols. Observed vertical gradients
of size-resolved number concentration within the canopy were reproduced only in the "gpc" scenario (Fig. 9b), although
other scenarios showed different tendencies as follows (Fig. 9c–e). When only dry deposition processes were considered (Fig.
9e), number concentration above the canopy was always larger than that within the canopy. Although the sharp negative
gradient of number concentration between height pairs was computed for the 0.1 - 0.4 μm size range when the gas-particle
conversion process was added to the model (Fig. 9d), positive gradients for large aerosols (> 0.2 μm) took on excessively high

values compared to observational data. The number concentration of such large aerosols increased within the canopy due to

305 hygroscopic growth (Fig. 9d and e), resulting in the negative gradient from the air above the canopy to the air within the canopy.

5.3 Impacts of gas-particle conversion and aerosol dynamics on dry deposition

To quantify the impact of gas-particle conversion of NH_4NO_3 on fine NO_3^- flux above the canopy, we plotted the respective ratios of HNO_3, NO_3^- and NH_4^+ fluxes over the canopy in the "gpc" scenario (F_{gpc}) to those in the "no gpc" scenario (F_{nogpc}), plotting each such ratio against RH in the early autumn period (Fig. 10). As depicted in Fig. 10b, the gas-aerosol equilibrium

310 of HNO_3 and NO_3^- shifted toward the aerosol phase under high RH conditions. Conversely, under low RH conditions (< 80 %), most F_{gpc}/F_{nogpc} ratio values were higher than unity for fine NO_3^- concentration (Fig. 10b and e). The impact of NH_4NO_3 evaporation on fine NO_3^- flux was very strong just under the deliquescence relative humidity (DRH) of pure NH_4NO_3 of 61.8 %; the F_{gpc}/F_{nogpc} ratio reached $\sim$ 40 around RH = 50 % (Fig. 10b). Notably, the thermodynamic equilibrium model in SOLVEG calculates the mutual DRH, which should not be pure NH_4NO_3 aerosols. Such high values of (apparent) NO_3^- flux

315 have been observed in various forest types in Europe, as summarized in Nemitz (2015). These cases may be also affected by NH_4NO_3 evaporation near the surface.

Calculated HNO_3 flux decreased with decreasing RH, due to evaporation of NH_4NO_3 (Fig. 10a). Most values of the F_{gpc}/F_{nogpc} ratio for HNO_3 under dry conditions (RH < 80 %) were below 0.5, and even tended to be negative, i.e., emission from the forest to the atmosphere. Prior studies have found this same flux difference; deposition velocity of HNO_3 varies in

320 a range from 4 to 7 cm s^{-1} (Huebert and Robert, 1985; Meyers et al., 1989; Sievering et al., 2001). These velocities have often been found to be lower than theoretical maximum values or even negative, i.e., emission from the canopy (Pryor et al. 2002; Nemitz et al., 2004a). High HNO_3 concentrations were observed within the canopy with the appearance of upward HNO_3 flux over the canopy (Pryor et al., 2002), indicating the possibility of flux divergence due to NH_4NO_3 evaporation in the HNO_3–NH_3– NH_4NO_3 triad within the forest. This explanation has already been suggested by other studies (Harrison et

325 al., 1989; Sutton et al., 1993; Kramm and Dlugi, 1994; Müller et al., 1993).

NH_4^+ flux over the forest was less influenced than NO_3^- by gas-to-particle conversion (Fig. 5c, f; Fig. 6d). Because dry deposition rates of NH_3 were much lower than those of HNO_3, NH_3 evaporation had little opportunity to enhance deposition fluxes. In fact, the observed deposition trends for NH_3 and NH_4^+ were much weaker than those for HNO_3 and NO_3^-. Also, while the major counter-ion of NO_3^- was NH_4^+, that of NH_4^+ was not NO_3^- but SO_4^{2-}. Even though same count of molecules of

330 NH_3 and HNO_3 evaporated, the gross deposition rate of NH_4^+ appears to have been influenced mainly by $(NH_4)_2SO_4$ and/or NH_4HSO_4 as also suggested by Nemitz (2015). The effect of NH_4NO_3 equilibrium on NH_3 flux was even lower than on fine NH_4^+ (Fig. 4a) because the mass concentration of NH_3 was much higher.

5.4 Influencing the chemical transport modeling

Theoretical values of deposition velocity for sub-micron aerosols typically ranging from 0.1 - 1 cm s^{-1} may typically have no

335 substantial impact on surface concentrations in chemical transport models. However, as discussed in the previous subsection, high deposition velocity of fine NO_3^- due to evaporation in the forest (up to 40 times the above values) may effectively remove

nitrate aerosols from the atmosphere over the forest and leeward. If the aerosol dynamics and gas-particle conversion processes can be incorporated into the dry deposition scheme in chemical transport models, we could improve upon or even eliminate prior studies' overestimates of the surface concentration of fine NO_3^- (Kajino et al., 2013; Shimadera et al., 2014, 2018;

340 Morino et al., 2015; Sakurai et al., 2015). Hicks et al. (2016) found that in modeling deposition velocities of aerosols, the greatest uncertainty manifests in the range 0.1 - 1.0 μm. The cause of this uncertainty is still not convincingly established, although the differing treatments of some key aerosol deposition processes (e.g., turbulent diffusion) have been suggested by prior studies (Petroff and Zhang, 2010; Zhang and Shao, 2014). As demonstrated in Fig. 10b and c, evaporation of NH_4NO_3 under less humid conditions may play an important role for dry deposition of sub-micron aerosols.

345 ## 6 Conclusions

A new multi-layer land surface model fully coupled with dry deposition and aerosol dynamics was developed to evaluate the impact of NH_4NO_3-NH_3-HNO_3 conversion in temperate forests. The model was applied to field studies of mass and number concentration profiles in a Japanese mixed forest during autumn 2016. Four model scenarios with/without NH_4NO_3 equilibrium and/or aerosol water uptake were tested to quantify the impact of the above processes on dry deposition processes. While the

350 model overall successfully reproduced micrometeorological conditions within and above the canopy, measured profiles of mass concentrations of gases (HNO_3 and NH_3) and fine aerosols (NO_3^- and NH_4^+) within the canopy were reproduced only in the model including NH_4NO_3 equilibrium processes. For aerosol size distribution, the observed emission tendency of total number concentration from the canopy to the atmosphere was explained by a larger effect of within-canopy evaporation of NH_4NO_3 than hygroscopic growth. As a result, the removal flux of calculated fine NO_3^- from the air above the forest to the forest can

355 increase by up to 40 times under the DRH of pure NH_4NO_3. Similarly, the removal flux of calculated fine NH_4^+ can increase up to $\sim$ 10 times, though calculations for fine NH_4^+ fluctuate strongly with RH. Conversely, HNO_3 flux over the forest can decrease by 50 % or more due to NH_4NO_3 evaporation, as supported by prior studies. The processes of aerosol dynamics and NH_4NO_3-NH_3-HNO_3 conversion play a crucial role in the dry deposition of inorganic nitrogen aerosols in temperate forests. These processes can and should be incorporated into chemical transport models to improve the accuracy of total nitrate surface

360 concentrations. An aerosol dynamics - dry deposition scheme simplified from that of this study can be implemented in chemical transport models with high feasibility.

Data availability. The output data in this study are publicly accessible via contacting the first author.

Author contributions. GK developed the model with supports from MK, and performed the simulations using the data collected by KM, AS, and KT. GK prepared the manuscript with contributions from all co-authors.

365 *Competing interests.* We have no conflict of interest to declare.

Acknowledgements. We gratefully acknowledge the helpful comments and suggestions from Dr. Kentaro Hayashi at the National Institute for Agro-Environmental Sciences, Dr. Tatsuya Sakurai at Meisei University, Dr. Takeshi Izuta at Tokyo University of Agriculture and Technology, Dr. Satoru Miura at the Forestry and Forest Products Research Institute, and Drs. Makoto Tamura and Tetsuji Ito at Ibaraki University, Japan. Our thanks are also extended to Mr. Mao Xu at the Tokyo University of Agriculture and Technology, Japan, for his contribution to the
370 filter-pack measurements. This work was partly supported by a Grant-in-Aid for Scientific Research (16H02933 and 17H01868) and Leading Initiative for Excellent Young Researchers, provided by the Japan Society for the Promotion of Science and the Ministry of Education, Culture, Sports, Science and Technology.

References

Bae, S.Y., Jung, C.H., and Kim, Y.P.: Development of an aerosol dynamics model for dry deposition process using the moment method, Aerosol. Sci. Technol., 43, 6, 570-580, 2009.

Binkowski F. S., and Shankar, U.: The regional particulate model 1. Model description and preliminary results, J. Geophys. Res., 100, D12, 26191-26209, 1995.

Brost, R.A., Delany, A.C., and Huebert, B.J.: Numerical modeling of concentrations and fluxes of HNO_3, NH_3, and NH_4NO_3 near the surface, J. Geophys. Res., 93, 7137-7152, 1998.

Burba, G., Schmidt, A., Scott, R.L., Nakai, T., Kathilankal, J., Fratini, G., Hanson, C., Law, B., McDermitt, D.K., Eckles, R., Furtaw, M., and Velgersdyk, M.: Calculating CO_2 and H_2O eddy covariance fluxes from an enclosed gas analyzer using an instantaneous mixing ratio, Glob. Change Biol., 18, 385-399, 2012.

Deventer, M.J., Held, A., El-Madany, T.S., Klemm, O.: Size-resolved eddy covariance fluxes of nuclear to accumulation mode aerosol particles over a coniferous forest, Agric. For. Meteorol., 214-215, 328-340, 2015.

Duarte, H. F., Dias, N.L. and Maggiotto, S.R.: Assessing daytime downward longwave radiation estimates for clear and cloudy skies in southern Brazil, Agric. For. Meteorol., 139, 171–181, 2006.

EANET (Acid Deposition Monitoring Network in East Asia): The Third Periodic Report on the State of Acid Deposition in East Asia Part III: Executive Summary, 2-5, https://www.eanet.asia/wp-content/uploads/2019/03/3_ex.pdf., 2016.

Farquhar, G.D., Firth, P.M., Wetselaar,R. and Weir, B.: On the gaseous exchange of ammonia between leaves and the environment: determination of the ammonia compensation point, Plant Physiol., 66, 710-714,1980.

Fowler, D., Pilegaard, K., Sutton, M.A., Ambus, P., Raivonen, M., Duyzer, J., Simpson, D., Fagerli, H., Fuzzi, S., Schjoerring, K.J., Granier, C., Nefter, A., Isaksen, I. S.A., Laj, P., Maione, M., and Monks, P.S.: Atmospheric composition change: Ecosystems-atmosphere interactions, Atmos. Environ., 43, 5193-5267, 2009.

Fountoukis, C., and Nenes, A.: ISORROPIA II: A computationally efficient thermodynamic equilibrium model for K^+-Ca^{2+}-Mg^{2+}-NH_4^+-Na^+-SO_4^{2-}-NO_3^--Cl^--H_2O aerosols, Atmos, Chem. Phys, 7, 4639–4659, 2007.

Harrison, R.M., Rapsomanikis, S. and Turnbull, A.: Land Surface Exchange in a Chemically-Reactive System - Surface Fluxes of HNO_3, HCl and NH_3, Atmos. Environ., 23, 1795-1800, 1989.

Harrison, R.M., Sturges, W.T., Kitto, A.M.N. and Li, Y.: Kinetics of the evaporation of ammonium chloride and ammonium nitrate aerosols, Atmos. Environ., 24A, 1883-1888, 1900.

Hicks, B. B., Saylor, R.D. and Baker, B.D.: Dry deposition of particles to canopies—A look back and the road forward, J. Geophys. Res. Atmos., 121, 14, 691-14, 707, doi:10.1002/2015JD024742.,2016.

Honjo, T., Takahashi, A. and Matsuda, K.: Deposition velocity of sulfate and nitrate in PM2.5 above a forest in suburban Tokyo using relaxed eddy accumulation, J. Jpn. Soc. Atmos. Environ., 51, 257-265, 2016 (in Japanese with English abstract).

Huebert, B.J., Luke, W.T., Delany, A.C. and Brost, R.A.: Measurements of concentrations and dry surface fluxes of atmospheric nitrates in the presence of ammonia, J. Geophys. Res., 93, 7127-7136, 1988.

Horst, T.W. and Lenschow, D.H.: Attenuation of scalar fluxes measured with spatially-displaced sensors, Bound.-Layer Meteorol., 130, 275-300, 2009.

Ibrom, A., Dellwik, E., Flyvbjerg, H., Jensen, N.O. and Pilegaard, K.: Strong low-pass filtering effects on water vapor flux measurements with closed-path eddy correlation systems, Agric. For. Meteorol., 147, 140-156, 2007.

410 Järvinen, A., Aitomaa, M., Rostedt, A., Keskinen, J., Yli-Ojanperä, J.: Calibration of the new electrical low pressure impactor (ELPI+), J. Aerosol Sci., 69, 150-159, 2014.

Kaimal, J.C. and Finnigan, J.J.: Atmospheric boundary layer flows: their structure and measurement, Oxford university press, 289, 1994.

Kajino, M., Inomata, Y., Sato, K., Ueda, H., Han, Z., An, J., Katata, G., Deushi, M., Maki, T., Oshima, N., Kurokawa, J., Ohara, T., Takami, A. and Hatakeyama, S.: Development of an aerosol chemical transport model RAQM2 and predications of Northeast Asian aerosol mass,
415 size, chemistry, and mixing type, Atmos. Chem. Phys., 12, 11833-11856, 2012.

Kajino, M., Sato, K., Inomata, Y. and Ueda, H.: Source–receptor relationships of nitrate in Northeast Asia and influence of sea salt on the long-range transport of nitrate, Atmos. Environ., 9, 67-78, 2013.

Katata, G.: Improvement of a land surface model for accurate prediction of surface energy and water balances, JAEA-Data/Code, 2008-033, 64, 2009.

420 Katata, G., Hayashi, K., Ono, K., Nagai, H., Miyata, A. and Mano, M.: Coupling atmospheric ammonia exchange process over a rice paddy field with a multi-layer atmosphere-soil-vegetation model, Agric. For. Meteorol., 180, 1-21, 2013.

Katata, G., Kajino, M., Matsuda, K., Takahashi, A. and Nakaya, K.: A numerical study of the effects of aerosol hygroscopic properties to dry deposition on a broad-leaved forest, Atmos. Environ., 97, 501-510, 2014.

Katata, G. and Ota, M.: A terrestrial ecosystem model (SOLVEG) coupled with atmospheric gas and aerosol exchange processes, JAEA-
425 Data/Code, 2016-014, 35, 2017.

Katata, G., Mauder, M., Zeeman, M., Grote, R. and Ota, M.: Wintertime carbon uptake of managed temperate grassland ecosystems may influence grassland dynamics, Biogeosci. Discuss., submitted.

Kramm, G. and Dlugi, R.: Modelling of the vertical fluxes of nitric acid, ammonia and ammonium nitrate, J. Atmos. Chem., 319-357, 1994.

Massad, R.-S., Nemitz, E. and Sutton, M.A.: Review and parameterisation of bi-directional ammonia exchange between vegetation and the
430 atmosphere, Atmos. Chem. Phys., 10, 10359-10386, 2010.

Matsuda, K., Watanabe, I., Mizukami, K., Ban, S. and Takahashi, A.: Dry deposition of PM2.5 sulfate above a hilly forest using relaxed eddy accumulation, Atmos. Environ., 107, 255-261, 2015.

Mauder, M. and Foken, T.: Impact of post-field data processing on eddy covariance flux estimates and energy balance closure, Meteorologische Zeitschrift, 15, 597-609, 2006.

435 Moncrieff, J.B., Clement, R., Finnigan, J. and Meyers, T.: Averaging, detrending and filtering of eddy covariance time series, in Handbook of micrometeorology: a guide for surface flux measurements, eds. Lee, X., Massman, W.J., Law, B.E.. Kluwer Academic, Dordrecht, 7-31, 2004.

Morino, Y., Nagashima, T., Sugata, S., Sato, K., Tanabe, K., Noguchi, T., Takami, A., Tanimoto, H. and Ohara, T.: Verification of chemical transport models for PM2.5 chemical composition using simultaneous measurement data over Japan, Aerosol Air Qual. Res., 15,
440 2009–2023, 2015.

Müller, H., Kramm, F. Meixner, Dollard, G.J., Fowler, D. and Possanzini, M.: Determination of HNO_3 dry deposition by modified bowen-ratio and aerodynamic profile techniques, Tellus B, 45, 346-367, 1993.

Nagai, H.: Atmosphere-soil-vegetation model including CO_2 exchange processes: SOLVEG2, JAERI-Data/Code, 2004-014, 92, 2004.

Nakahara, S., Takagi, K., Sorimachi, A., Katata, G. and Matsuda, K.: Enhancement of dry deposition of PM2.5 nitrate in a cool-temperate
445 forest, Atmos. Environ., 212, 136-141, 2019.

Nemitz, E. and Sutton, M.A.: Gas-particle interactions above a Dutch heathland: III. Modelling the influence of the NH_3-HNO_3 − NH_4NO_3 equilibrium on size-segregated particle fluxes, Atmos. Chem. Phys., 4, 1025-1045, 2004.

Nemitz, E., Sutton, M.A., Wyers, G.P., Otjes, R.P., Mennen, M.G., van Putten, E.M. and Gallagher, M.W.: Gas-particle interactions above a Dutch heathland: II. Concentrations and surface exchange fluxes of atmospheric particles, Atmos. Chem. Phys., 4, 1007-1024, 2004.

450   Nemitz, E.: Surface/atmosphere Exchange of Atmospheric Acids and Aerosols, Including the Effect and Model Treatment of Chemical Interactions. Review and Integration of Biosphere-Atmosphere Modelling of Reactive Trace Gases and Volatile Aerosols, Springer, 115–149, 2015.

Neirynck, J., and Ceulemans, R.: Bidirectional ammonia exchange above a mixed coniferous forest, Environ. Pollut., 154, 424-438, 2008.

Ota, M., Nagai, H. and Koarashi, J.: Root and dissolved organic carbon controls on subsurface soil carbon dynamics: A model approach, J.

455   Geophys. Res., 118, 1646-1659, 2013.

Petroff, A. and Zhang, L.: Development and validation of a size-resolved particle dry deposition scheme for application in aerosol transport models, Geosci. Model Dev., 3, 753-769, 2010.

Pryor, S.C., Barthelmie, R.J., Jensen, B., Jensen, N.O. and Sørensen, L.L.: HNO_3 fluxes to a deciduous forest derived using gradient and REA methods, Atmos. Environ., 36, 5993-5999, 2002.

460   Sakamoto, T., Nakahara, A., Takahashi, A., Sorimachi, A., Katata, G. and Matsuda, K.: Deposition velocity of PM2.5 nitrate and gaseous nitric acid above a forest in suburban Tokyo using relaxed eddy accumulation with denuder sampling technique, J. Jpn. Soc. Atmos. Environ, 53, 136-143, 2018 (in Japanese with English abstract).

Sakurai, T., Satake, S. and Matsuda, K.: Measurement of the inorganic ions in PM2.5 at western Tokyo and the evaluation for AQM performance based on the measurement, Earozoru Kenkyu, 30, 134-141, 2015 (In Japanese with English abstract).

465   Shimadera, H., Hayami, H., Chatani, S., Morino, Y., Mori, Y., Morikawa, T., Yamaji, K. and Ohara, T.: Sensitivity analyses of factors influencing CMAQ performance for fine particulate nitrate, J. Air Waste Manage. Assoc., 64, 374-387, 2014.

Shimadera, H., Hayami, H., Chatani, S., Morikawa, T., Morino, Y., Mori, Y., Tamaji, K., Nakatsuka, S. and Ohara, T.: Urban air quality model inter-comparison study (UMICS) for improvement of PM2.5 simulation in greater Tokyo area of Japan, Asian J. Atmos. Environ, 12, 139-152, 2018.

470   Sievering, H., Enders, G., Kins, L., Kramm, G., Ruoss, K., Roider, G., Zelger, M., Anderson, l. and Dlugi, R.: Nitric acid, particulate nitrate and ammonium profiles at the Bayerisher Wald: evident for large deposition rates of total nitrate, Atmos. Environ., 28, 311-315, 1994.

Sutton, M.A., Pitcairn, C.E.R. and Fowler, D.: The exchange of ammonia between the atmosphere and plant communities, Adv. Ecol. Res., 24, 301-393, 1993.

Takahashi, A. and Wakamatsu, T.: Estimation of deposition velocity of particles to a forest using the concentration gradient method, J. Jpn.

475   Soc. Atmos. Environ., 39, 53-61, 2004 (In Japanese with English abstract).

van Hove, L.W.A., Adema, E.H. and Vredenberg, W.J.: A study of the adsorption of NH_3 and SO_2 on leaf surfaces, Atmos. Environ., 23, 1479-1486, 1989.

van Oss, R., Duyzer, J., and Wyers, P.: The influence of gas-to-particle conversion on measurements of ammonia exchange over forest, Atmos. Environ., 32, 465-471, 1998.

480   Vickers, D. and Mahrt, L.: Quality control and flux sampling problems for tower and aircraft data, J. Atmospheric Ocean. Technol., 14, 512-526, 1997.

Wolff, V., Meixner, F.X. and Trebs, I.: Mixing ratios and exchange processes of the ammonia-nitric acid-ammonium nitrate triad above a spruce forest canopy. In: H. Lacoste-Francid (Ed.), Earth Observations for Land-Atmosphere Interaction Science. European SpaceAgency, ESTEC PO Box 299 2200, 2011.

485 Yamazaki, T., Takahashi, A. and Matsuda, K.: Differences of dry deposition between sulfate and nitrate in PM2.5 to a forest in suburban Tokyo by vertical profile observations, J. Jpn. Soc. Atmos. Environ., 50, 167-175, 2015 (In Japanese with English abstract).

Zhang, Q., Jimenez, J.L., Canagaratna, M.R., D. Allan, J.D., Coe, H., Ulbrich, I., Alfarra, M., Takami, A., Middlebrook, A.M., Sun, Y.L., Dzepina, K., Dunlea, E., Docherty, K., DeCarlo, P., Salcedo, D., Onasch, T., Jayne, J.T., Miyoshi, T., Shimono, A. and Worsnop, D.: Ubiquity and dominance of oxygenated species in organic aerosols in anthropogenically-influenced Northern Hemisphere midlatitudes,
490 Geophys. Res. Lett., 34, L13801, doi:10.1029/2007GL029979, 2007.

Zhang, J. and Shao, Y.: A new parameterization of particle dry deposition over rough surfaces, Atmos. Chem. Phys., 14, 12429-12440, 2014.
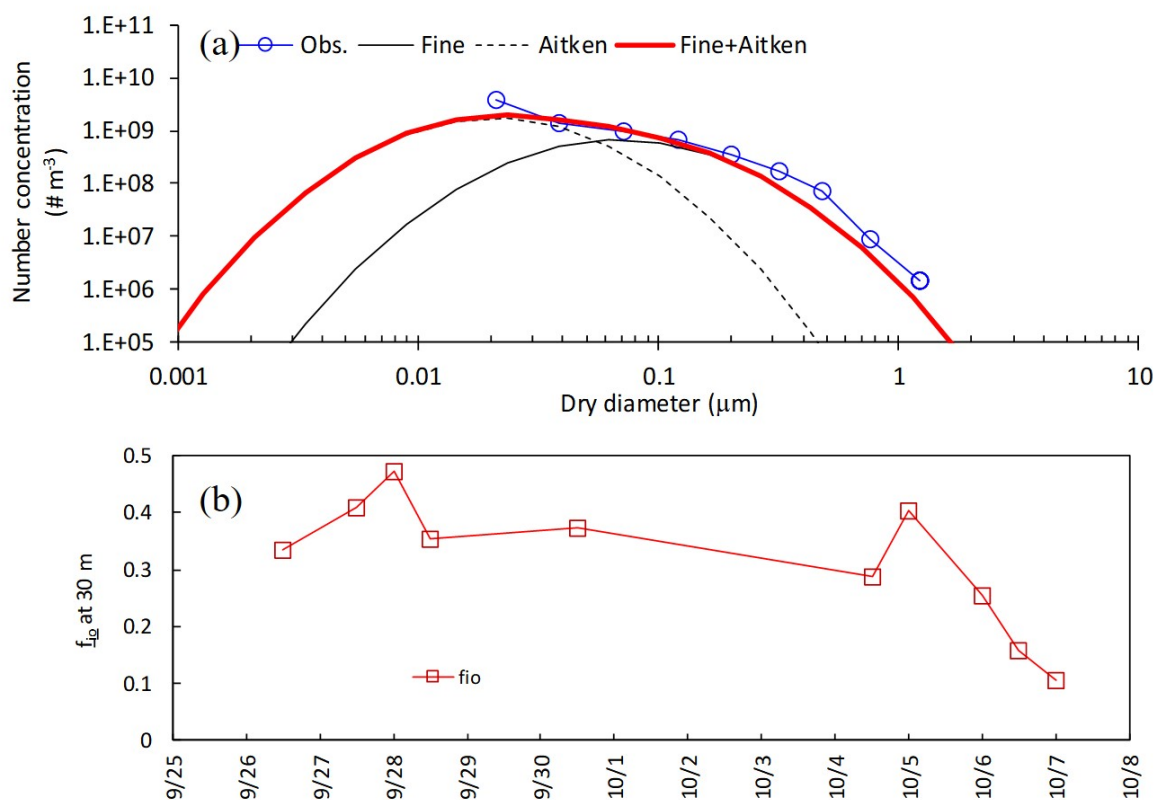
Figure 1. (a) Modeled and observed number-based size distribution of aerosols at 10:00 on 7 November 2016, and (b) temporal changes in the volume fraction of inorganic compounds (f_{io}) in the early autumn period.
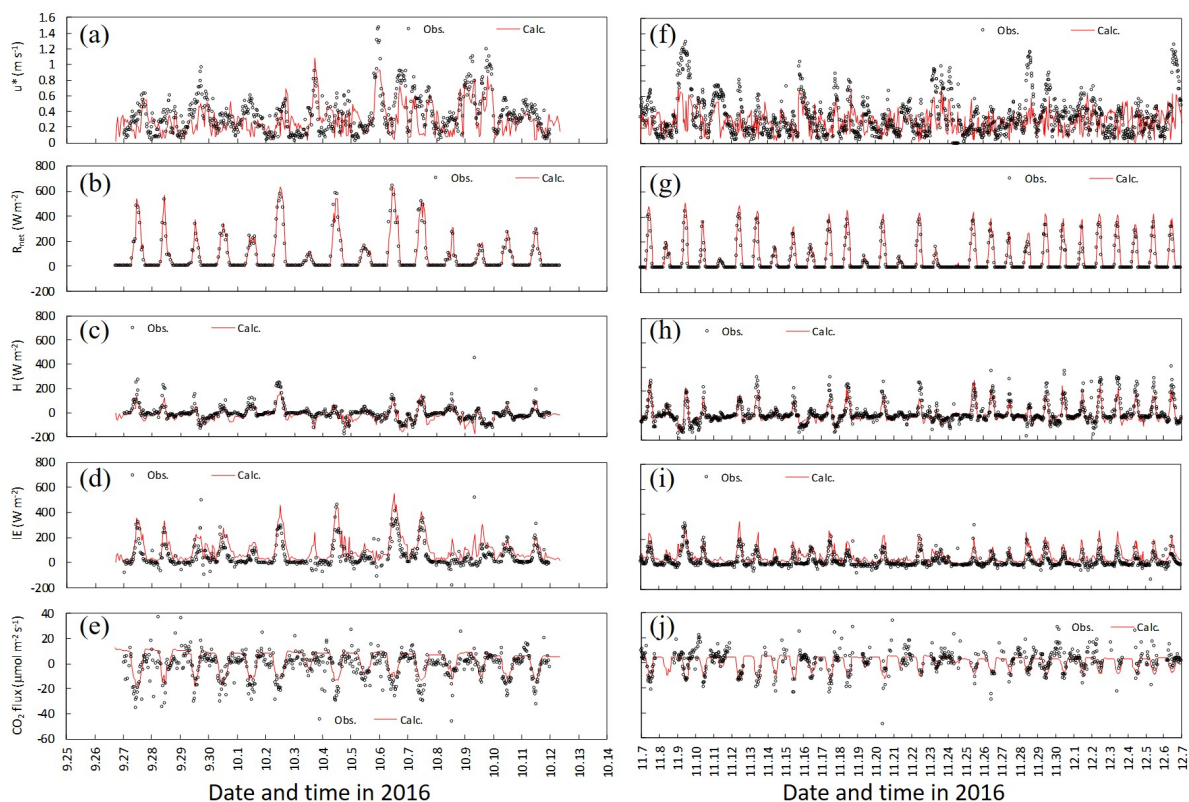
Figure 2. Temporal changes in observed and simulated (a, f) friction velocity, (b, g) net radiation, (c, h) sensible and (d, i) latent heat, and (e, j) CO_2 fluxes (a–e) from 27 September to 11 October and (a–e) from 7 November to 6 December 2016.
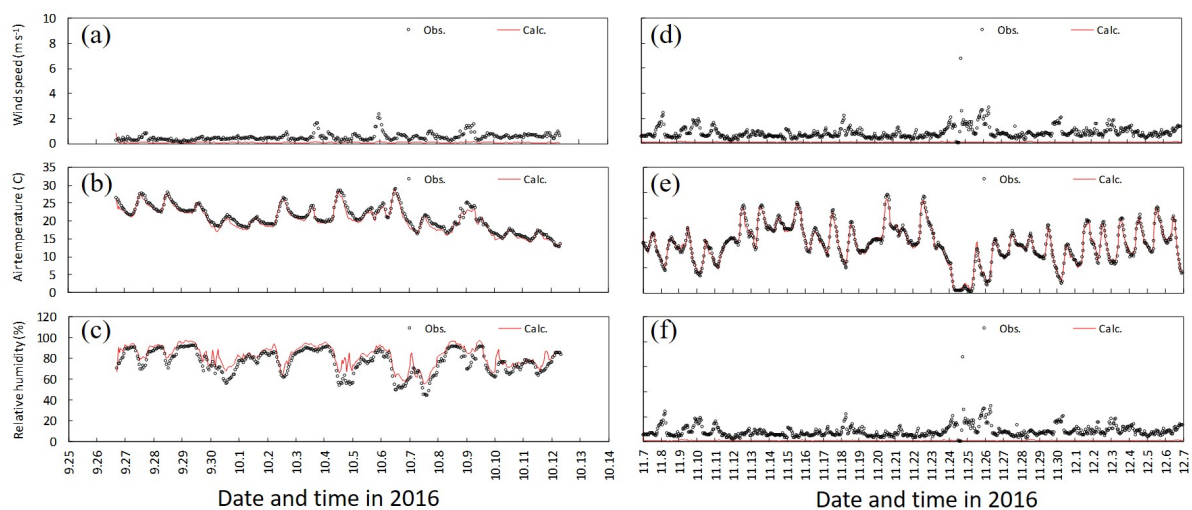
Figure 3. Temporal changes in observed and simulated (a, d) horizontal wind speed, (b, e) air temperature, and (c, f) relative humidity at 6 m height (a–c) from 27 September to 11 October and (d–f) from 7 November to 6 December 2016.
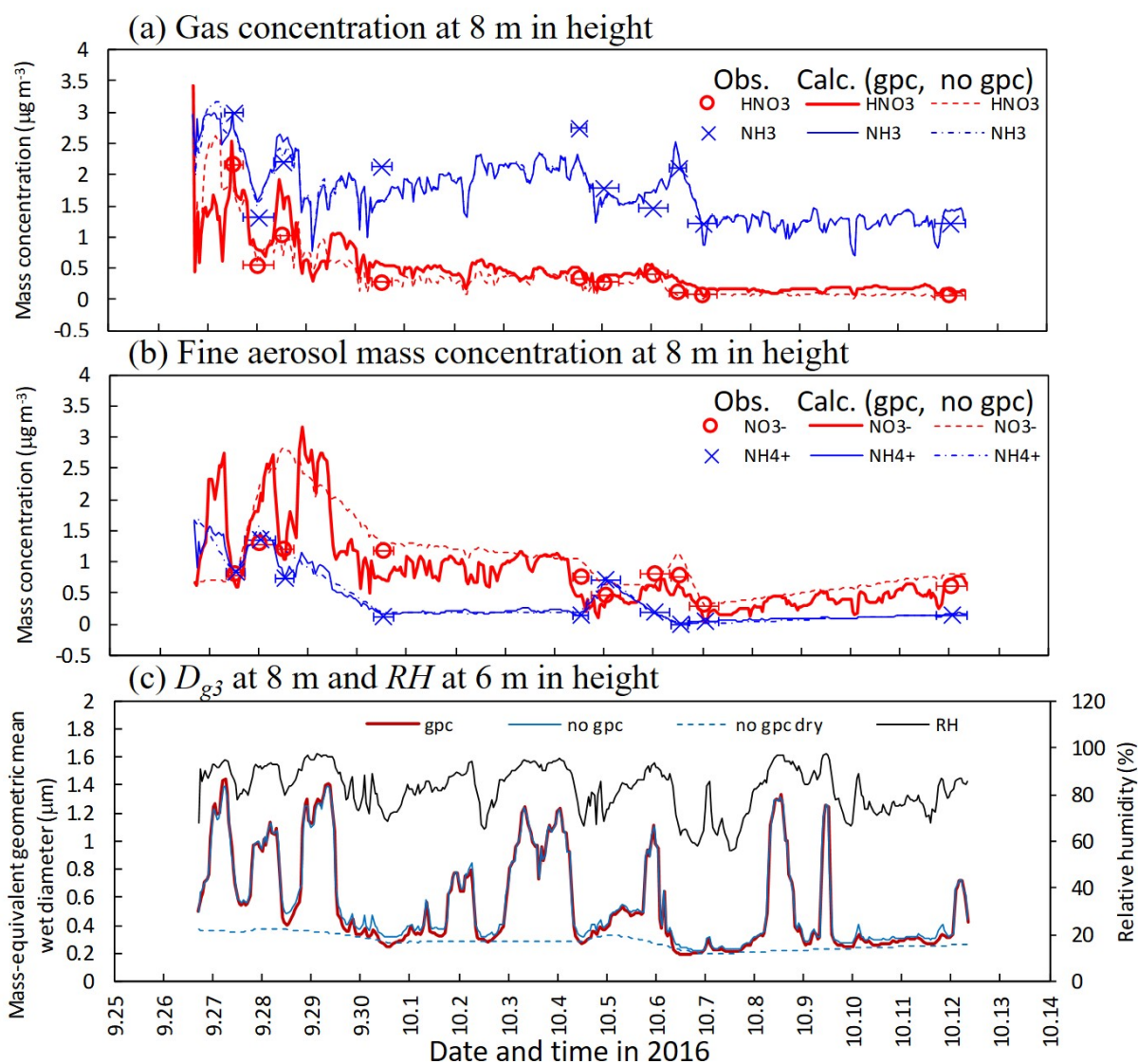
Figure 4. Temporal changes in observed and calculated mass concentrations of (a) HNO_3 and NH_3 gases and (b) NO_3^- and NH_4^+ fine aerosols, and mass-equivalent geometric mean wet diameter (D_{g3}) at 8 m height from 27 September to 11 October 2016. Calculations for three scenarios ("gpc", "no gpc", and "no gpc dry") are plotted in the figure. Calculated relative humidity (RH) at 6 m height in Fig. 3c also appears in (c).
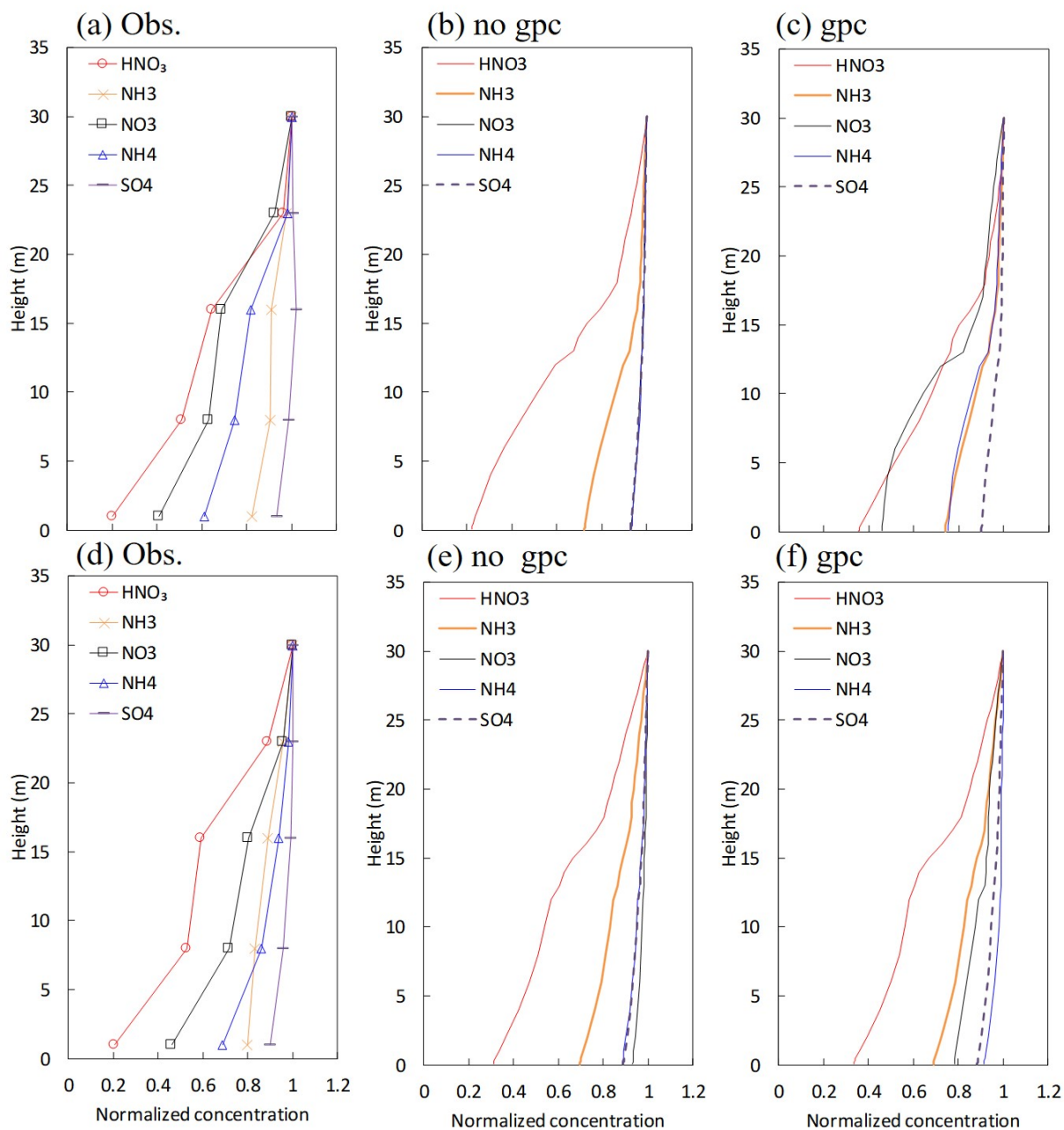
Figure 5. Mean vertical profiles in (a) observed and (b) calculated normalized mass concentration in the "no gpc" scenario and (c) the "gpc" scenario for HNO_3 and NH_3 gases and SO_4^{2-}, NO_3^- and NH_4^+ fine aerosols (a–c) during the daytime and (d–f) nighttime from 27 September to 11 October 2016.
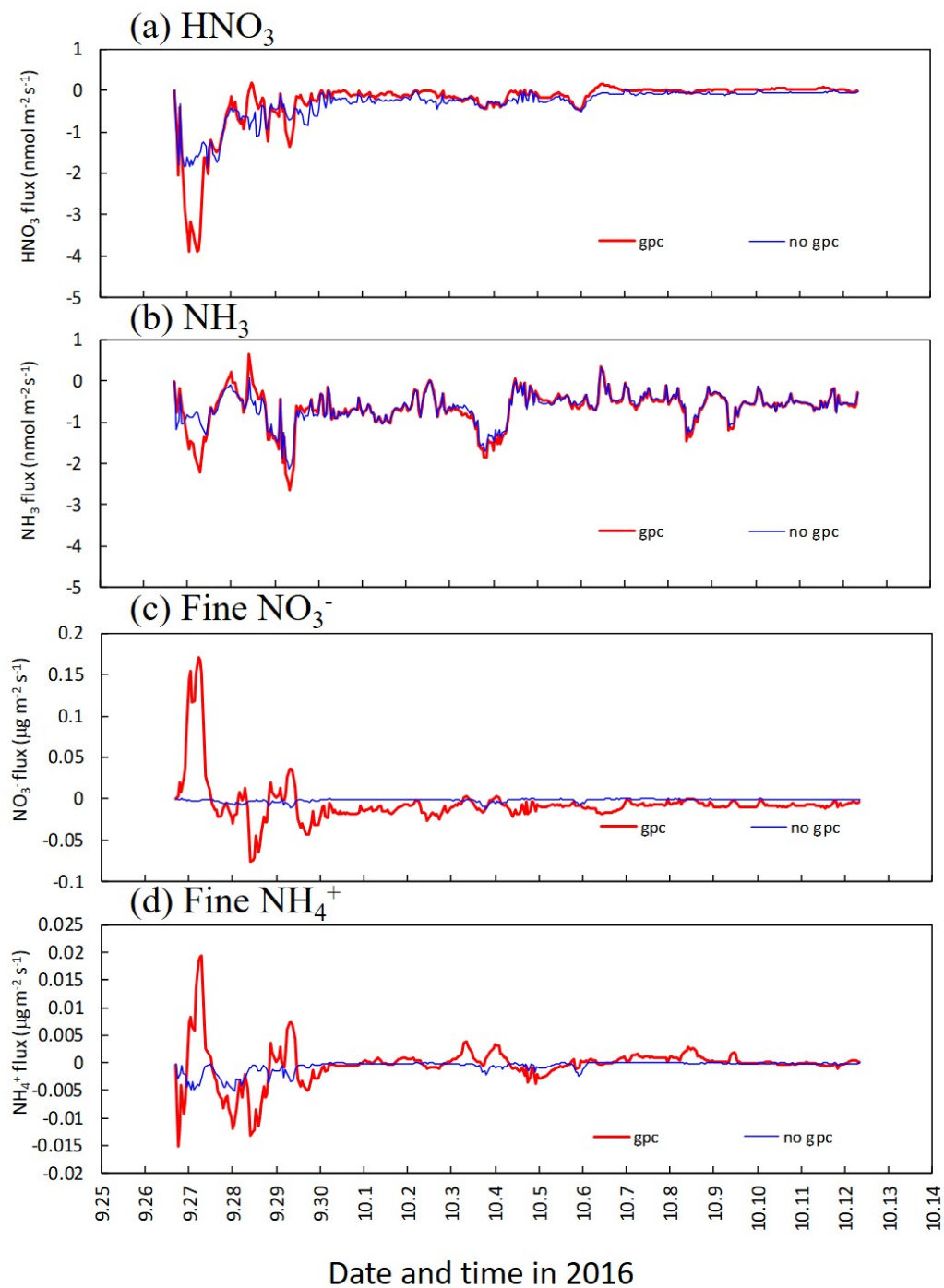
Figure 6. Temporal changes in calculated mass flux of (a) HNO_3 gas and (b) NO_3^- and NH_4^+ fine aerosols from 27 September to 11 October 2016. Calculations in two scenarios ("gpc" and "no gpc") are plotted in the figure.
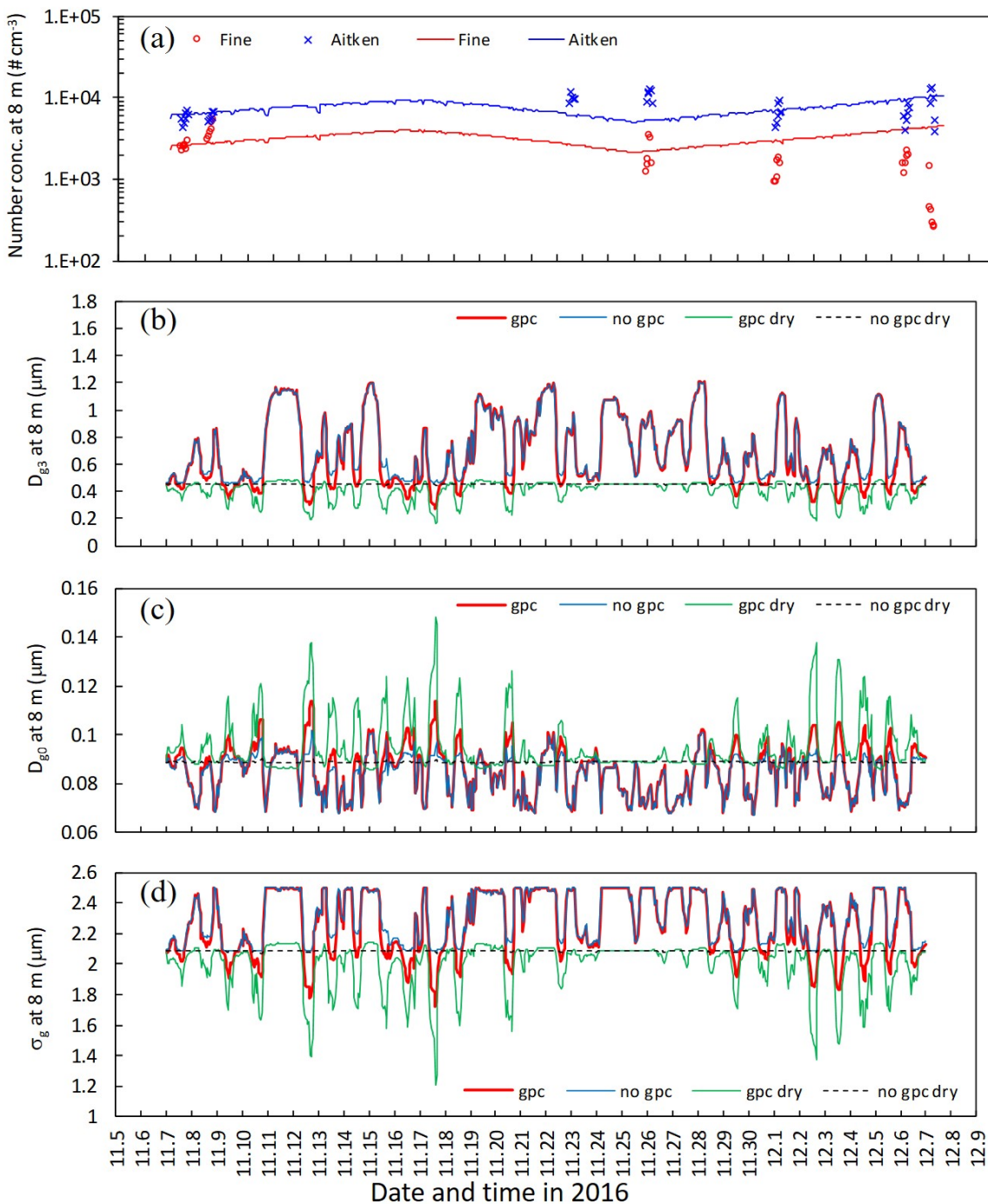
Figure 7. Temporal changes in (a) observed and calculated number concentration of fine and Aitken modes, and (b) calculated mass-equivalent (D_{g3}) and (c) number-equivalent geometric mean wet diameter (D_{g0}), and (d) standard deviation (σ_g) of fine aerosols at 8 m height from 7 November to 7 December 2016. Calculations for four scenarios ("gpc", "no gpc", "gpc dry", and "no gpc dry") are plotted in the figure.
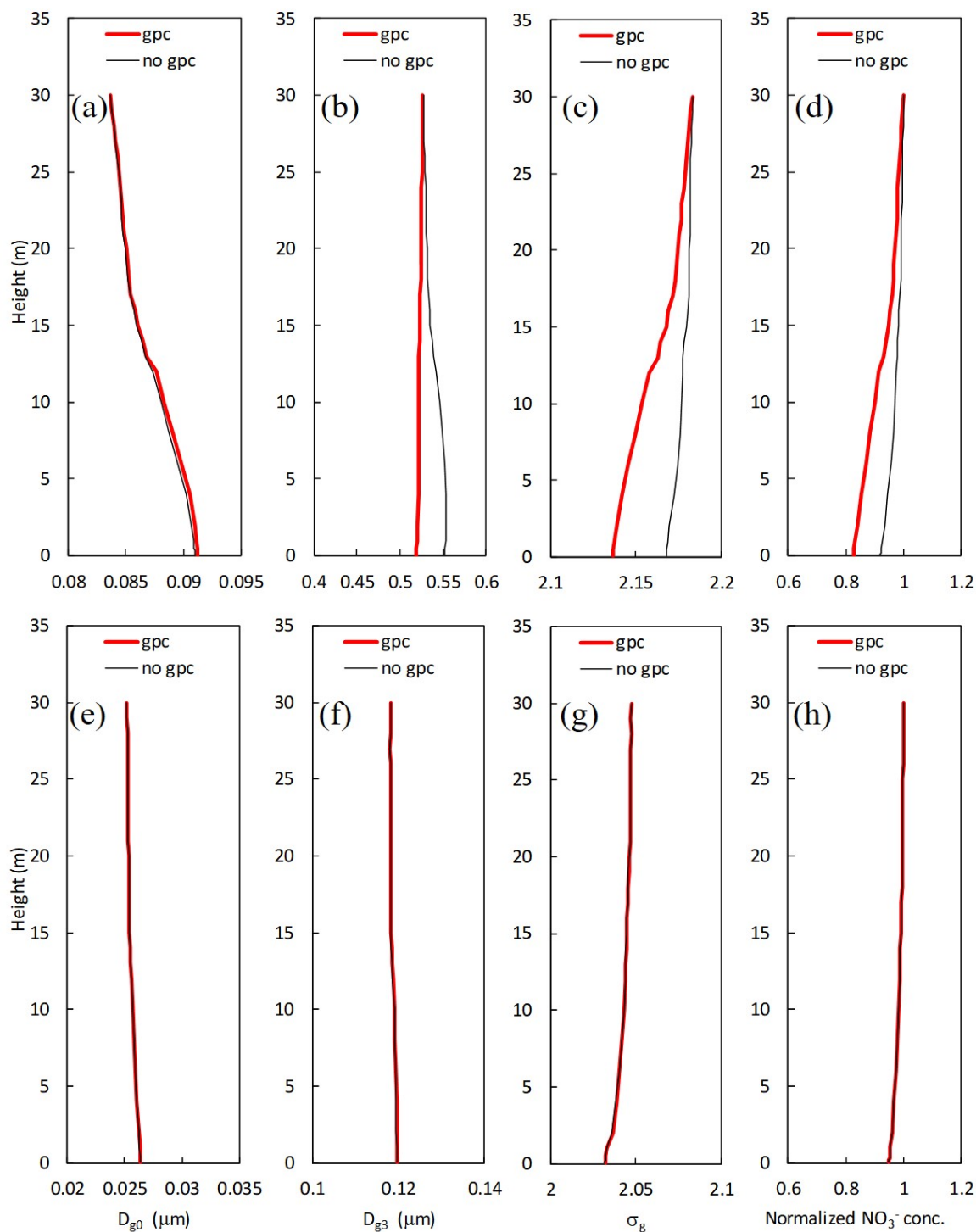
Figure 8. Mean vertical profiles for calculated (a, e) number-equivalent (D_{g0}) and (b, f) mass-equivalent geometric mean wet diameter (D_{g3}), (c, g) standard deviation (σ_g), and (d, h) normalized mass concentration of NO_3^- for (a–d) fine and (e–h) Aitken modes in two scenarios ("gpc" and "no gpc") from 7 November to 7 December 2016.
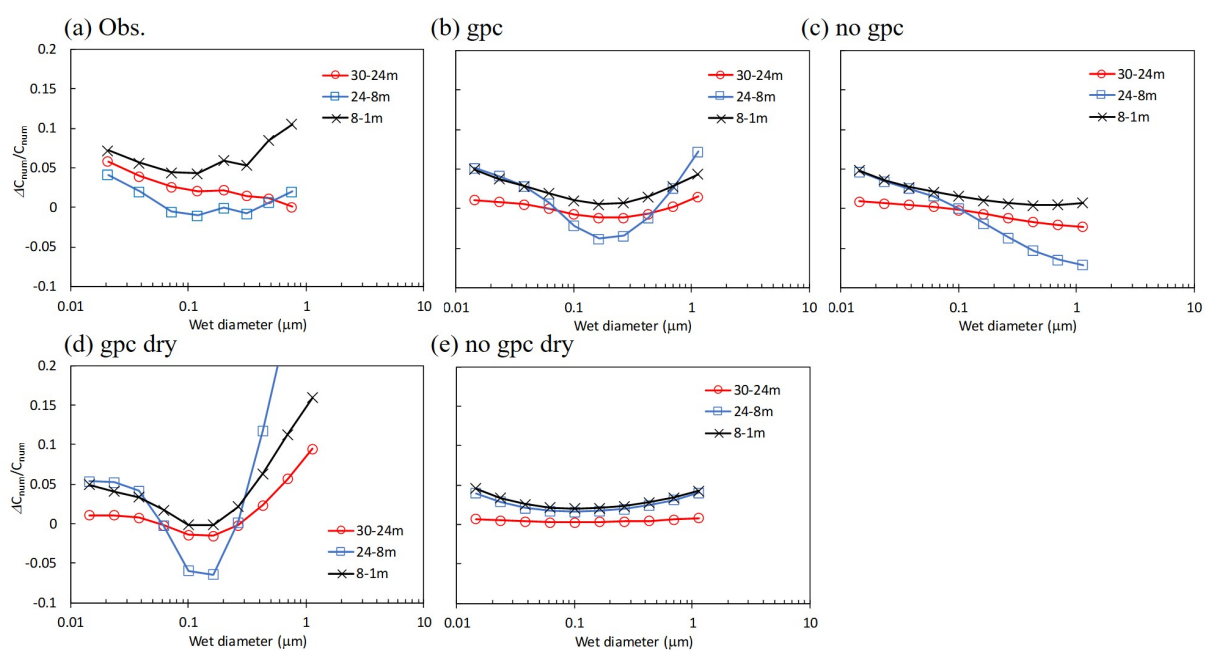
Figure 9. Differences in (a) observed and (b–e) calculated mean total number concentration between height pairs for 11:00 –17:00 on 7, 8, 25, and 30 November 2016. Four calculation scenarios are presented in the figure: (b) "gpc", (c) "no gpc", (d) "gpc dry", and (e) "no gpc dry".
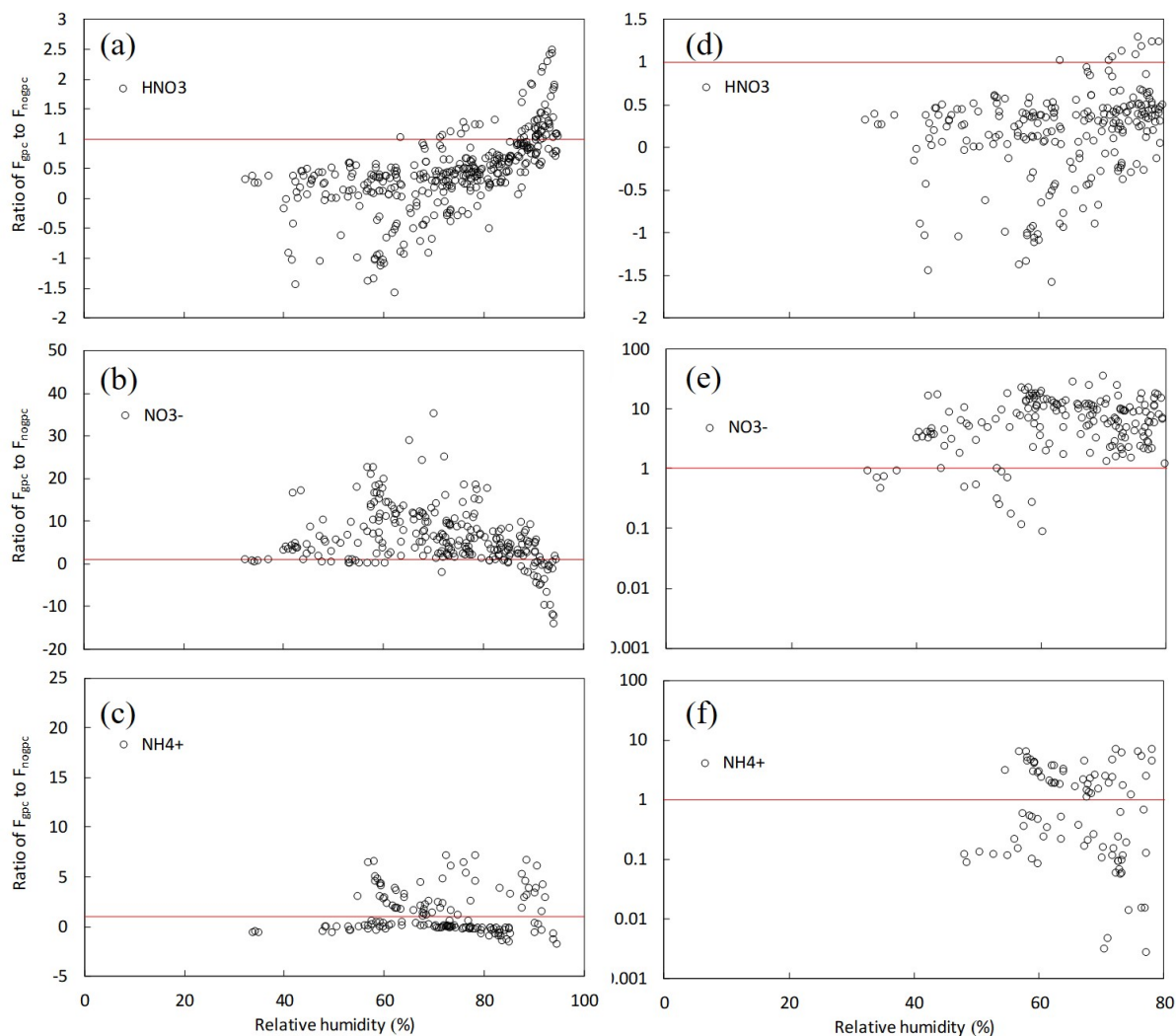
Figure 10. Relationship between relative humidity (RH) at 30 m height and "gpc" to "no gpc" ratios of calculated half-hourly fluxes (F_{gpc}/F_{nogpc}) of (a, d) HNO$_3$ gas and (b, e) NO$_3^-$ and (c, f) NH$_4^+$ fine aerosols over the canopy from 27 September to 11 October 2016. Red lines represent the situation in which $F_{gpc} = F_{nogpc}$. (d) through (f) plot the same variables as (a) through (c), but under dry conditions ($RH < 80$ %).